Clay Minerals, (2018) **53**, 17–28

Infrared and Mössbauer spectroscopy of Fe-rich smectites from Morrón de Mateo bentonite deposit (Spain)

M. PELAYO[1,*], J. F. MARCO[2], A. M. FERNÁNDEZ[1], L. VERGARA[2], A. M. MELÓN[1] AND L. PÉREZ DEL VILLAR[1]

[1] *Department of Environment, CIEMAT, Avenida Complutense 40, 28040 Madrid, Spain*
[2] *Institute of Physical Chemistry Rocasolano, CSIC, Calle Serrano 119, 28006 Madrid, Spain*

(*Received 9 September 2016; revised 15 September 2017; Associate Editor: Juan Cornejo*)

ABSTRACT: The Morrón de Mateo bentonite deposit has been studied as a natural analogue of the thermal effect on the bentonite barrier of a geological radioactive waste repository. This deposit was intruded by a volcanic dome that induced hydrothermal activity affecting the smectite clay minerals close to the dome. Previous studies of proximal bentonites indicated that Al-montmorillonites were transformed into Fe-rich smectites with intermediate composition between beidellite and saponite through gradual steps formed by smectites increasingly rich in Mg and Fe. In order to confirm the suggested transformation and the Fe distribution into the smectites, infrared and Mössbauer spectroscopy studies were performed. Infrared spectra of samples away from the dome show typical bands for montmorillonite type with prevailing Al in octahedral positions, while proximal samples also show bands of Fe-rich smectites. Mössbauer data confirm that Fe present in the fine fraction of bentonites is fundamentally located in the smectites structure, mainly as octahedrally coordinated Fe(III). Proximal smectites have a considerably more distorted octahedral environment for Fe(III) which probably stemmed from a significant degree of substitution of Al by Fe(III). These results confirm that an alteration process occurred related to the volcanic intrusion which produced an increase in temperature and Fe-rich solutions responsible for the transformation of Al-montmorillonites.

KEYWORDS: Fe-rich smectites, bentonite barrier, natural analogues, infrared and Mössbauer spectroscopic techniques.

In the framework of the Spanish programme on the deep geological disposal of high-level radioactive wastes, the Morrón de Mateo bentonite deposit has been studied as a natural analogue of the bentonite barrier behaviour after burial, in relation to the thermal and geochemical effects induced by the radioactive decay of the fission products and the interaction between the corrosion products from the steel canister and the bentonite, respectively. This bentonite deposit, including its host rocks and the overlying biocalcarenite beds, was intruded by a rhyodacitic volcanic dome which induced a metasomatic process by means of hydrothermal Fe-Mg-rich fluids, mainly manifested by the transformation of calcite from the biocalcarenite beds into Fe-Mg-rich dolomite in the zone nearest to the dome (Delgado, 1993; Pérez del Villar *et al*., 2005). Based on those results, the present authors carried out a mineralogical, chemical, geochemical and isotopic study of the smectites from the bentonite deposit in order to verify whether these bentonites were also affected by the aforementioned metasomatic process. Smectites located away from the dome were found to

*E-mail: m.pelayo@ciemat.es
https://doi.org/10.1180/clm.2018.1

be dioctahedral Al-rich smectites, similar to those from other deposits in the region (Reyes, 1977; Caballero *et al*., 1985; Delgado, 1993), while smectites located in the vicinity of the dome are a mixture of Al-montmorillonites, Fe-rich montmorillonites and beidellites, and intermediate smectites, between beidellite and Fe-rich saponite (Pelayo, 2014; Pelayo *et al*., 2016). Furthermore, the textural relationships observed by Scanning Electron Microscopy (SEM), coupled with an Energy Dispersive X-ray spectroscopy (EDX) system, suggested that the smectites with intermediate composition come from the gradual transformation of Al-montmorillonite to smectites with increasing Mg and Fe contents (Pelayo, 2014; Pelayo *et al*., 2016). To confirm this suggestion, smectites located distant from and close to the sub-volcanic dome were studied by infrared (FTIR) and Mössbauer spectroscopy to analyse the Fe distribution in the fine fractions of bentonite. The main goal of the present study was to understand and confirm the transformation processes that occurred in the smectites from the Morrón de Mateo deposit as a result of their interaction with the hydrothermal Fe-Mg-rich fluids related to the intrusion of the rhyodacitic volcanic dome.

Infrared spectroscopy is a very efficient method for studying the distribution of cations in the structure of phyllosilicates, especially in the octahedral sheet, as the OH bands are sensitive to both structural and compositional variations (Farmer, 1974; Madejová *et al*., 1994; Russell & Fraser, 1994; Bishop *et al*., 2002). The IR region corresponding to both OH-stretching and bending vibrational modes provides qualitative and quantitative information about cation distribution in the octahedral sheet (Vantelon *et al*., 2001).

Mössbauer spectroscopy allows determination of the oxidation state of Fe in phyllosilicates, oxides and other Fe-rich minerals or admixtures, and, in favourable cases, also the Fe coordination, making this technique suitable for the characterization of their Fe-compounds (Coey, 1980; Goodman, 1994; Murad, 2010). Additionally, because the quadrupole splitting of Fe(III) is determined by external charges, its magnitude provides a direct indication of the site distortion (Murad, 2010). On the other hand, this spectroscopic technique allows distinction between Fe bound in oxides and in clay mineral structures, and also identification of the Fe-oxyhydroxide species present in the samples (Murad, 1988, 2010; Komadel *et al*., 1999).

Furthermore, in laboratory experiments performed to study the stability of the bentonite barrier, as a consequence of its interaction with corrosion products of the Fe-rich container, both FTIR and Mössbauer spectroscopic techniques are usually employed to quantify the amount of the destabilized smectite, resulting from the interaction with Fe, which allows the comparison with the original smectite (Guillaume *et al*., 2004; Lantenois *et al*., 2005; Wilson *et al*., 2006).

GEOLOGICAL SETTING

The Morrón de Mateo deposit is the main bentonite mass in the vicinity of the volcanic dome known as Morrón de Mateo. It is located in the central sector of the Cabo de Gata region (Almería), specifically in the Escullos depression, which is placed between the Frailes volcanic structure, to the south, and the Rodalquilar Caldera Complex, to the north. The deposit forms part of a Lower Tortonian volcano-sedimentary series (11.6 Ma), which mainly consists, from the bottom to the top, of the following geological units: (1) hornblende-rich andesitic breccias; (2) bentonitized pyroclastic layered rocks (White Tuffs formation); (3) marine sedimentary rocks; and (4) partially bentonitized epiclastic rocks (Mass Flow formation) (Fig. 1), which have been described extensively by Fernández-Soler (2002). The Morrón de Mateo dome intruded through this volcano-sedimentary series. The White Tuffs formation is the main host and parent rock of the bentonite deposit and is composed of a succession of white-coloured, soft layers of bentonite-rich tuffs and tabular layers of a brownish to greenish sandy material, poorer in smectite, that form base surge and co-surge hydromagmatic facies. This formation shows some sedimentary structures that point to lateral currents as the main transport and deposition mechanism. These features suggest that the white-layered tuffs may have formed as a result of phreatomagmatic activity triggered by magma–water interaction in a shallow marine environment, probably in a depressed coastal embayment (Fernández-Soler, 1992).

MATERIALS AND METHODS

Materials

Fourteen representative samples from the White Tuffs Formation, previously characterized by X-ray diffraction (XRD) (Pelayo, 2014), were selected for FTIR analysis. They were collected from eight boreholes. Three samples (S2, S3 and S4) are located away from the volcanic dome (distal samples), in the

https://doi.org/10.1180/clm.2018.1 Published online by Cambridge University Press

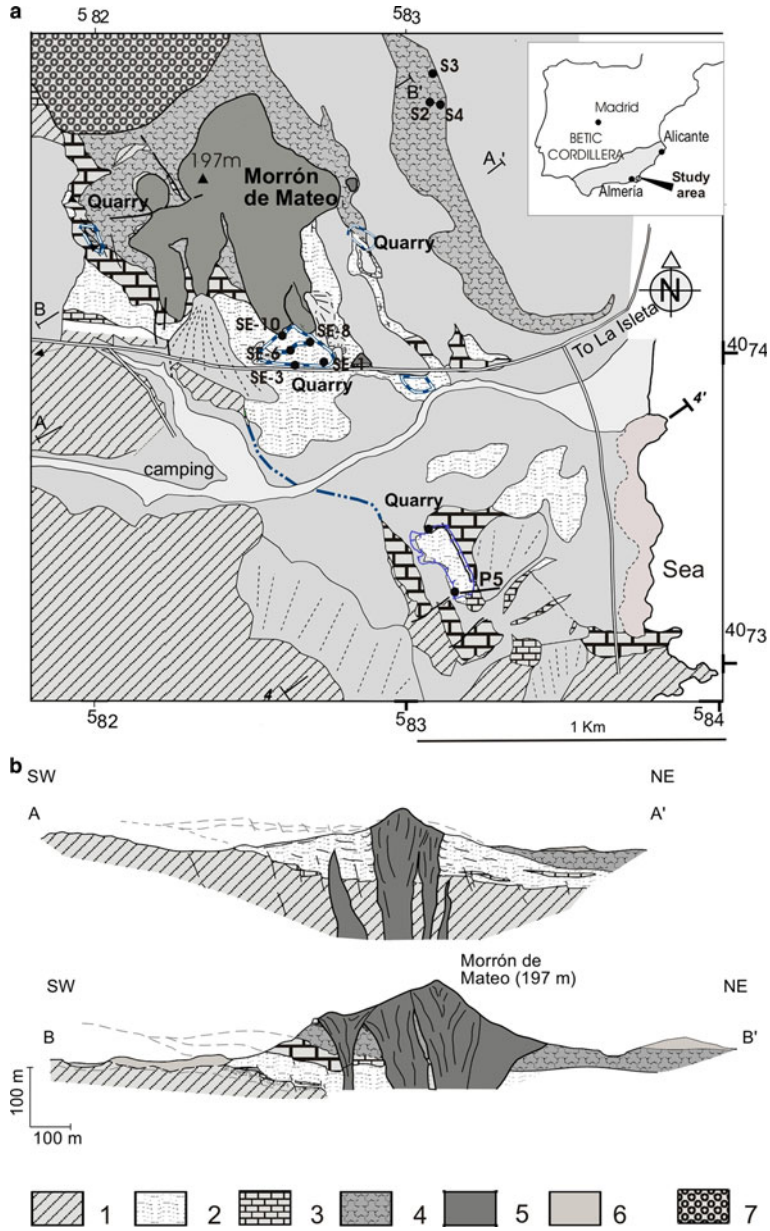

FIG. 1. (a) Geological map of the Morrón de Mateo area with the studied boreholes (S2, S3, S4, SE-1, SE-3, SE-6, SE-8 and SE-10) and profile (P5) (modified after Fernández-Soler, 2002). (b) Geological cross-sections A–A' and B–B' showing the relationship between the sub-volcanic intrusion and the volcano-sedimentary sequence. Key: (1) hornblende-rich andesite breccias; (2) White Tuffs formation; (3) Tortonian biocalcarenite beds; (4) Mass flow formation; (5) Morrón de Mateo dome; (6) Quaternary sediments; (7) Rodalquilar complex rhyodacitic rock.

northeast zone of the Morrón de Mateo area, and the remaining samples (SE-1, SE-3, SE-6, SE-8 and SE-10) are located close to the dome (proximal samples), in the quarry to the south of the dome. The depth of the boreholes varies from 15 to 33 m. One other sample was taken from a surface cross-section (P5) located far from the dome, in the so-called El Murciano quarry (Fig. 1, Table 1). In addition, four samples from

https://doi.org/10.1180/clm.2018.1 Published online by Cambridge University Press

Table 1. Sample locations, depth and technique used in their study.

Samples	Borehole/profile	Location	Depth (m)	Technique
MTO-14	Profile P5	Distal (1120 m from the dome)	–	FTIR; Mössbauer
S2M10	Borehole S2	Distal (750 m from the dome)	13.5	FTIR
S3M10	Borehole S3	Distal (800 m from the dome)	14.6	FTIR
S4M4	Borehole S4	Distal (800 m from the dome)	7.7	FTIR
SE1M7	Borehole SE-1	Proximal	6.9	FTIR; Mössbauer
SE1M16		Proximal	14.9	FTIR
SE3M12	Borehole SE-3	Proximal	9.8	FTIR
SE3M26		Proximal	22.9	FTIR
SE6M10	Borehole SE-6	Proximal	11.4	FTIR
SE6M19		Proximal	20.1	FTIR; Mössbauer
SE8M3	Borehole SE-8	Proximal	4.0	FTIR
SE8M6		Proximal	7.2	FTIR; Mössbauer
SE10M12	Borehole SE-10	Proximal	10.0	FTIR; Mössbauer
SE10M23		Proximal	18.7	FTIR

proximal boreholes (SE-1, SE-6, SE-8 and SE-10) and one sample from the distal surface profile (P5) were selected for Mössbauer spectroscopy (Table 1).

The < 2 μm fractions used in this study were from the White Tuffs formation, extracted by conventional sedimentation method (Moore & Reynolds, 1997).

Sample description

Detailed characterization of the samples was reported by Pérez del Villar *et al.* (2005), Pelayo *et al.* (2011), Pelayo (2014) and Pelayo *et al.* (2016). The fine fraction (<2 μm) of bentonite samples from the White Tuffs formation, located both close to and

Table 2. Mineralogical composition (%) of the < 2 μm fraction from distal and proximal samples, characterised by XRD.

Sample	Smectite	Illite	Cristobalite	Zeolites	Di/Tri
MTO-14	89	0	11	0	Di
S2M10	96	0	4	0	Di
S3M10	94	Tr	Tr	6	Di
S4M4	100	0	0	Tr	Di
SE1M7	99	0	Tr	0	Di/tri
SE1M16	100	0	0	0	Di
SE3M12	97	0	3	0	Di/tri
SE3M26	99	0	Tr	0	Di
SE6M10	99	0	Tr	Tr	Di/tri
SE6M19	99	0	Tr	Tr	Di/tri
SE8M3	99	Tr	Tr	Tr	Di/tri
SE8M6	96	Tr	2	2	Di/tri
SE10M12	99	Tr	Tr	Tr	Di/tri
SE10M23	99	Tr	Tr	Tr	Di/tri

Tr: traces; Di/Tri: existence of dioctahedral and trioctahedral smectite.

https://doi.org/10.1180/clm.2018.1 Published online by Cambridge University Press

TABLE 3. Structural formulae of smectites (calculated from TEM and EDX data) from distal samples (numbers of cations on the basis of O_{20} $(OH)_4$).

	Tetrahedral		Octahedral			Interlayer		
Sample	Si	Al^{IV}	Al^{VI}	Fe(III)	Mg	Ca	K	Na
MTO-14	7.92	0.08	2.56	0.44	1.29	0.08	0.27	0.06
S2M10	7.91	0.10	2.63	0.42	1.21	0.16	0.07	0.15
S3M10	7.91	0.09	2.53	0.47	1.21	0.16	0.22	0.12
S4M4	7.86	0.14	2.56	0.52	1.22	0.13	0.05	0.18

away from the volcanic dome, consists mainly of dioctahedral smectite with minor illite, zeolites and cristobalite. The coexistence of dioctahedral and trioctahedral or intermediate di-trioctahedral smectite has been observed in some proximal samples (Table 2).

The structural formulae of smectites from distal samples (Table 3) correspond to Al-rich montmorillonites because of the prevalence of octahedral charge and the octahedral occupancy ranging from 4.21 to 4.33 cations per unit cell (p.u.c.).

The smectites from proximal samples (Table 4) have a broader compositional variability. Thus, two groups were differentiated on the basis of their chemical composition: (1) Al-rich smectites, which are the more abundant in all the samples; and (2) Mg-Fe-rich smectites. The Al-rich smectites have mainly octahedral charge, except for samples SE1M7 and SE10M12 with a prevalence of tetrahedral charge. Furthermore, the number of Fe(III) cations is generally larger than that shown by distal smectites, with values > 0.6 p.u.c. in some samples, classifying them as Fe-rich montmorillonites or beidellites (Brigatti, 1983). In summary, five proximal samples (SE1M16, SE3M12, SE3M26, SE6M10 and SE6M19) are Al-montmorillonites, three (SE8M3, SE8M6 and SE10M23) are Fe-rich montmorillonites and two (SE1M7 and SE10M12) are Fe-rich beidellites.

The structural formulae of smectites with high Fe and Mg contents present in three representative proximal samples (SE3M12, SE8M3 and SE10M12)

TABLE 4. Structural formulae of smectites (calculated from TEM and EDX data) from proximal samples (numbers of cations on the basis of O_{20} $(OH)_4$).

	Tetrahedral		Octahedral			Interlayer		
Sample	Si	Al^{IV}	Al^{VI}	Fe(III)	Mg	Ca	K	Na
SE1M7	7.60	0.4	2.22	0.89	1.24	0.12	0.09	0.29
SE1M16	7.95	0.05	2.64	0.54	1.04	0.16	0.07	0.00
SE3M12	7.96	0.04	2.56	0.46	1.23	0.14	0.05	0.16
SE3M12 (Mg-Fe smectite)	7.03	0.97	0.77	1.54	2.76	0.10	0.0	0.26
SE3M26	7.76	0.24	2.50	0.53	1.26	0.15	0.07	0.25
SE6M10	7.95	0.05	2.43	0.53	1.29	0.17	0.11	0.11
SE6M19	7.78	0.22	2.41	0.53	1.34	0.17	0.07	0.30
SE8M3	7.65	0.35	2.31	0.71	1.26	0.08	0.21	0.38
SE8M3 (Mg-Fe smectite)	7.01	0.99	0.82	1.51	2.59	0.08	0.11	0.58
SE8M6	7.83	0.17	2.26	0.80	1.19	0.11	0.11	0.19
SE10M12	7.48	0.52	2.61	0.65	1.06	0.12	0.12	0.19
SE10M12 (Mg-Fe smectite)	6.61	1.40	0.91	1.53	2.78	0.14	0.02	0.20
SE10M23	7.72	0.28	2.32	0.72	1.22	0.19	0.12	0.23

https://doi.org/10.1180/clm.2018.1 Published online by Cambridge University Press

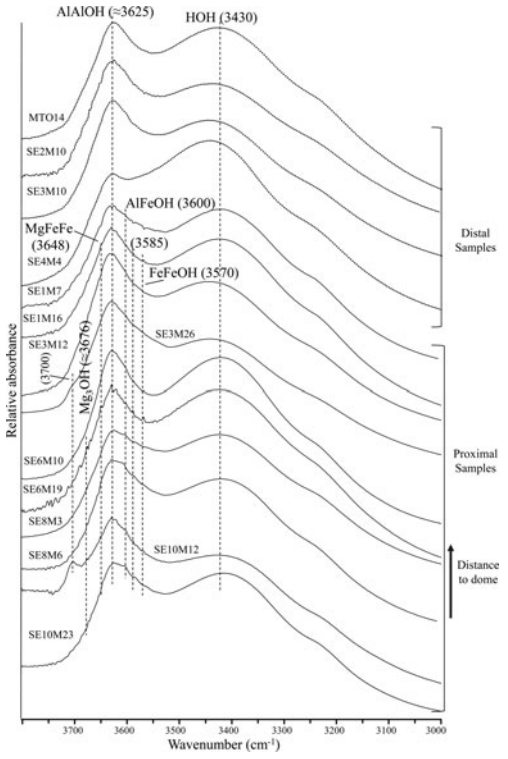

FIG. 2. FTIR spectra of distal and proximal samples in the OH-stretching region.

are listed in Table 4. They show a prevalence of tetrahedral charge and octahedral occupancy ranging from 4.91 to 5.22 cations p.u.c.. Mg is the main octahedral cation, followed by Fe(III) and Al. Therefore, these smectites may be classified as intermediates between beidellite and Fe-rich saponite.

Methodology

A Fourier transform infrared (FTIR) spectroscopic study was carried out using a Nicolet 6700 FTIR spectrometer equipped with a DTGS detector and a KBr beam splitter, at a resolution of 4 cm^{-1}, in transmission mode. 1 mg of sample was mixed with 200 mg of KBr to obtain pellets after pressing (10 tons max. load). The spectra per pellet sample were collected before and after heating at 110°C for 24 h in order to remove most of the adsorbed water. Analyses were carried out at room temperature in the Pore Water Chemistry Laboratory of the Environment Department, CIEMAT. The spectra were recorded in the mid-IR region (MIR), in the range 4000 to 400 cm^{-1}. The OH-stretching region between 3800 and 3200 cm^{-1} and the OH-bending region between 1000 and 750 cm^{-1} were studied in detail.

Mössbauer spectra were recorded at room temperature (300 K) in transmission mode, using a constant acceleration spectrometer and a ^{57}Co (Rh) source. An effective absorber thickness of approximately 5–10 mg Fe/cm^2 was used in all cases. The velocity scale was calibrated using a 12 μm thick Fe foil and the isomer shifts were referred to the centroid of the spectrum of α-Fe at room temperature. With the aim of identifying the presence of Fe-oxyhydroxides, spectra were also recorded at 16 K for two samples using a closed-cycle He-cooled cryostat. The widths and areas of the two lines of a particular quadrupole doublet were assumed to be equal and those of the sextets had their areas held to a 3:2:1:1:2:3 ratio.

RESULTS AND DISCUSSION

Infrared spectroscopy

The FTIR spectra of the distal and proximal samples are shown in Fig. 2. The spectra show two main absorption bands in the OH-stretching region: one near 3625 cm^{-1}, which is attributed to the AlAlOH vibration, typical of dioctahedral Al-rich smectites (Farmer, 1974); and a broader band at 3430 cm^{-1}, assigned to the OH-stretching vibration due to molecular water absorption (Zviagina *et al*., 2004).

Furthermore, two shoulders near 3600 cm^{-1} and 3570 cm^{-1} are observed in most of the proximal samples. These bands correspond to AlFeOH and FeFeOH vibrations, respectively, of Fe-rich smectites (Bishop *et al*., 1999; Komadel *et al*., 1999; Madejová *et al*., 2000; Petit *et al*., 2002). In addition, two weak shoulders near 3676 cm^{-1} and 3648 cm^{-1} are noted mainly in the proximal samples SE6M19 and SE10M12. The first shoulder is attributed to Mg_3OH stretching vibrations of saponite (Farmer, 1974; Van der Marel & Beutelspacher, 1976; Parra *et al*., 1985), while the second may correspond to $MgFe_2OH$ stretching modes of Fe-rich saponites. Iron substitution in saponite shifts the Mg_3OH stretching band towards a lower frequency (Wilkins & Ito, 1967; Russell & Fraser, 1994; Cuadros *et al*., 2008). The existence of such bands is consistent with the presence of smectite with intermediate composition between beidellite and Fe-rich saponite in the proximal samples, in accordance with the structural formula calculations from TEM + EDX data (Table 3) (Pelayo, 2014; Pelayo *et al*., 2016).

https://doi.org/10.1180/clm.2018.1 Published online by Cambridge University Press

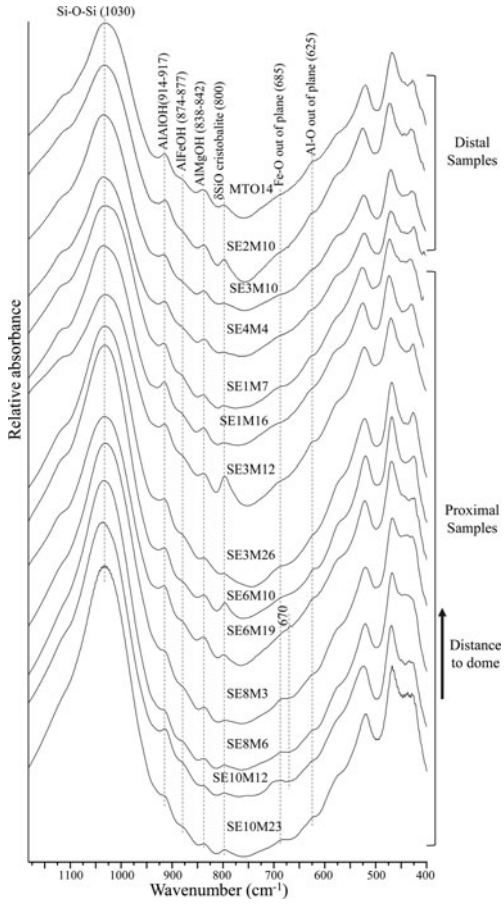

FIG. 3. FTIR spectra of distal and proximal samples in the OH-bending region.

Additionally, the band around 3700 cm^{-1} in the spectra from proximal samples SE3M26 and SE10M12 may be attributed to Mg_3OH vibrations in dehydrated saponites containing interlayer Na or K (Farmer, 1974), chlorite/smectite mixed-layers (Van del Marel & Beutelspacher, 1976; Bergaya *et al*., 1985) or to outer AlAlOH vibrations in kaolinite (Farmer, 1998; Madejová, 2003). As neither kaolinite nor chlorite/smectite mixed-layers was identified by XRD, the band at ~ 3700 cm^{-1} might be due to the presence of smectite with intermediate composition between beidellite and Fe-rich saponite, identified in sample SE10M12 (Pelayo, 2014).

In the region between 1050 and 1000 cm^{-1} (Fig. 3), a strong band appears at 1030 cm^{-1}, characteristic of Si-O vibrations of dioctahedral smectites (Goodman, 1976).

In the OH-bending region (Fig. 3), the three bands at 914-917 cm^{-1}, 874-877 cm^{-1} and 838-842 cm^{-1}, corresponding to AlAlOH, AlFeOH and AlMgOH vibrations of smectites (Farmer, 1974; Goodman *et al*., 1976; Russell & Fraser, 1994; Vantelon *et al*., 2001), are observed in all spectra. The AlFeOH vibration band is well defined in most proximal samples, and very weak in distal samples (Fig. 3). This indicates a higher Fe content in smectites from the proximal samples compared to their counterparts from distal samples, in agreement with the structural formulae (Table 3).

Furthermore, a band near 685 cm^{-1} appears in most of the proximal samples, which may correspond to out-of-plane OH-bending vibrations in Fe-rich smectites when the structure is disrupted by (1) tetrahedral substitution of Fe^{3+} for Si and/or octahedral cation substitution, or (2) by variations in hydroxyl position due to missing OH groups (Bishop *et al*., 2002). This band may be the out-of-plane bending vibrations predicted by Farmer (1974) and may represent small trioctahedral domains within the dioctahedral smectite.

A weak shoulder around 670 cm^{-1} is observed in samples SE6M19 and SE10M12 which is assigned to Mg_3OH vibrations in trioctahedral smectites (Farmer 1974). This fact, coupled with the presence of two shoulders near 3676 cm^{-1} and 3648 cm^{-1}, seems to confirm the existence of saponite in the samples.

Additionally, some samples have a band at 625 cm^{-1} which corresponds to Al–O out-of-plane bending vibrations of Al-rich smectites with structural disorder due to tetrahedral and/or octahedral substitution (Bishop *et al*., 2002). Finally, the relatively strong band at 800 cm^{-1} observed in most samples is assigned to a SiO-bending vibration in cristobalite (Madejová & Komadel, 2001), which was identified by XRD in the fine fractions of the samples (Table 2) (Pelayo, 2014).

Mössbauer spectroscopy

The Mössbauer spectra of the five samples studied are presented in Fig. 4. The Mössbauer parameters, the assignment to different Fe-species and their relative concentrations are listed in Table 5.

The Mössbauer spectrum of the distal sample MTO-14 recorded at 16 K is almost identical to that obtained at room temperature. Both spectra are dominated by an intense paramagnetic doublet (98% of the total spectral area) having Mössbauer parameters ($\delta = 0.32$ mm/s; $\Delta = 0.53$ mm/s) characteristic of Fe(III) in octahedral coordination (Bancroft *et al*., 1973). In addition, both

https://doi.org/10.1180/clm.2018.1 Published online by Cambridge University Press

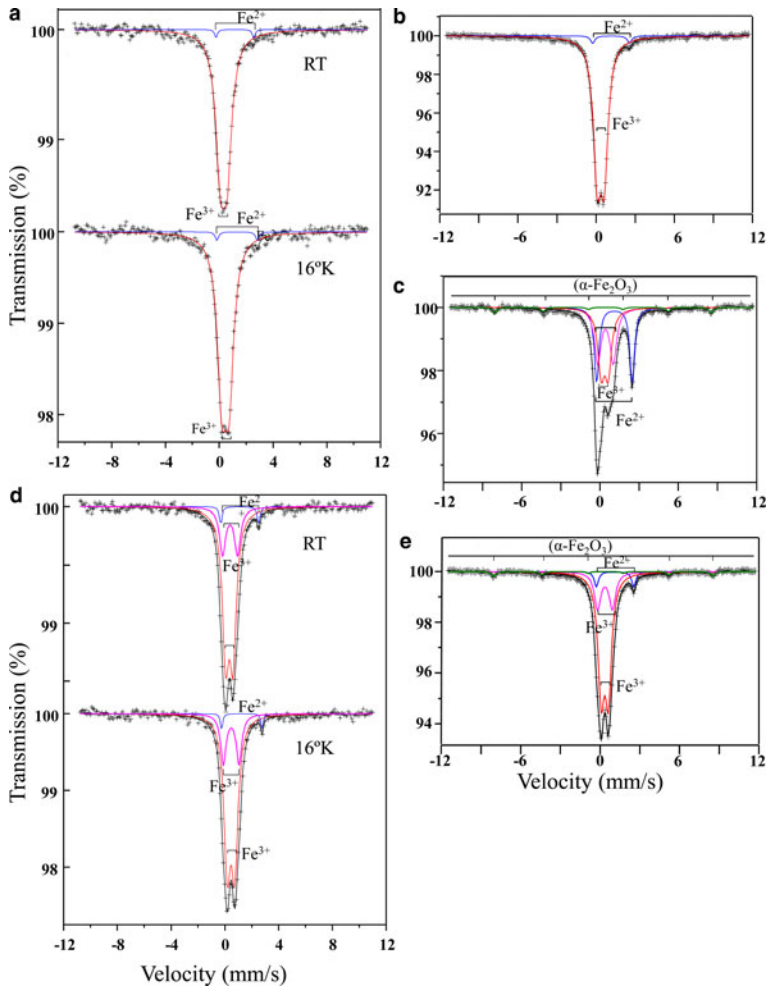

FIG. 4. Mössbauer spectra of the studied samples: (a) MTO-14 (distal); (b) SE1M7 (proximal); (c) SE6M19 (proximal); (d) SE8M6 (proximal); (e) SE10M12 (proximal); RT: room temperature (298 K).

spectra show an additional small doublet with parameters ($\delta = 1.10$ mm/s and $\Delta = 2.82$ mm/s) characteristic of Fe(II) in octahedral coordination (Bancroft *et al*., 1973). The absence of magnetic sextets at 16 K precludes the existence of Fe(III) oxides. Therefore, all the Fe(III) ions of the sample belong to the crystal structure of smectite.

The RT Mössbauer spectrum of the proximal sample SE1M7 is similar to that of the distal sample MTO-14, characterized by an intense paramagnetic doublet typical of Fe(III) in octahedral coordination, corresponding to 97% of the total Fe species and a small doublet, with parameters ($\delta = 1.15$ mm/s; $\Delta = 2.82$ mm/s), characteristic of Fe(II). The spectra of samples SE6M19, SE8M6 and SE10M12 have two doublets characteristic of octahedral Fe(III) with different quadrupole splitting value (Δ) (Table 5). One doublet has a quadrupole splitting value of approximately 0.55 mm/s, whilst the second has a quadrupole splitting value ranging between 1.11 and 1.18 mm/s. The much larger quadrupole splitting value indicates a considerably more distorted octahedral environment for these Fe(III) octahedral cations (Maddock, 1985).

Other authors (Coey, 1980; Heller-Kallai & Rozenson, 1981; De Grave *et al*., 1985) relate the two doublets with different quadrupole splitting values to Fe(III) ions in *cis*- and *trans*-octahedral sites. According to the diagram proposed by Coey (1980), the lower quadrupole splitting value is situated in the

https://doi.org/10.1180/clm.2018.1 Published online by Cambridge University Press

TABLE 5. Mössbauer parameters obtained from the fit of the spectra recorded from the samples studied (mm/s), assignment to different Fe-species and their relative concentrations.

		Fe(III) (VI) (A)			Fe(III) (VI) (B)			Fe(II) (VI)			α-Fe_2O_3			
Samples	T (°K)	δ (mm/s)	Δ (mm/s)	Area (%)	δ (mm/s)	Δ (mm/s)	Area (%)	δ (mm/s)	Δ (mm/s)	Area (%)	Δ (mm/s)	2ε (mm/s)	H (T)	Area (%)
MTO-14	300	0.32	0.53	98	–	–	–	1.10	2.82	2	–	–	–	–
Distal	16	0.46	0.53	98	–	–	–	1.30	3.00	2	–	–	–	–
SE1M7 Proximal	300	0.36	0.54	97	–	–	–	1.15	2.82	3	–	–	–	–
SE6M19 Proximal	300	0.36	0.53	34	0.42	1.18	31	1.10	2.72	31	0.33	−0.22	53.1	4
SE8M6 Proximal	300	0.33	0.55	74	0.39	1.11	22	1.10	2.82	4	–	–	–	–
	16	0.45	0.56	74	0.48	1.18	22	1.26	3.02	4	–	–	–	–
SE10M12 Proximal	300	0.36	0.54	69	0.38	1.12	22	1.13	2.82	6	0.33	−0.20	51.3	3

δ: Isomer shift; Δ: quadrupole splitting (in doublets); 2ε: quadrupole shift (in sextets); H: hyperfine magnetic field; (VI): octahedral coordination.

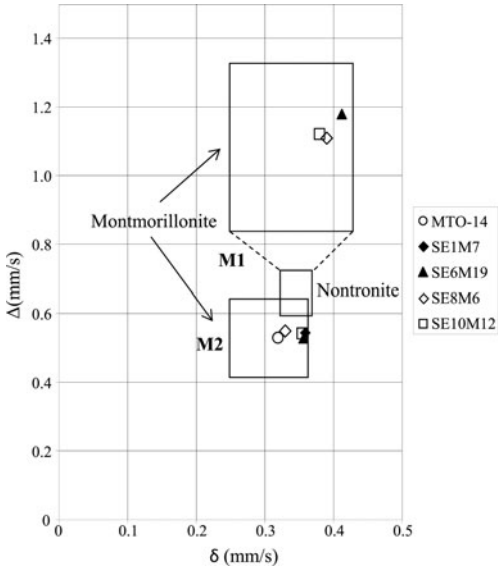

FIG. 5. Isomer shift (δ) *vs*. quadrupole splitting value (Δ) diagram proposed by Coey (1980). The M1 field corresponds to Fe (III) in octahedral *trans* positions, whilst the M2 field corresponds to Fe (III) in octahedral *cis* positions. The symbols correspond to the values of the samples studied in this work.

field of Fe(III) in *cis* positions (M2), while the higher value is located in the field of Fe(III) in *trans* positions (M1) (Fig. 5). Therefore, samples MTO-14 and SE1M7 with only one doublet might have Fe(III) in *cis* octahedral positions (M2). However, Cardile & Johnston (1986) suggested that Mössbauer doublets should not be assigned to *cis*- and *trans*-sites in the unit cell of 2:1 silicates, and this was further supported by independent studies which suggested that the observed differences of the quadrupole splitting are caused by a distortion of the Fe(III)-octahedron due to the different local structural and chemical environments (Dainyak & Drits, 1987; Dainyak *et al*., 1992). Furthermore, the substitution of Al by Fe(III) causes distortion of the octahedron due to the larger ionic radius of Fe(III) (Rozalén, 2004), which suggests that in the proximal samples a significant substitution of Al by Fe(III) in octahedral sheets took place. This fact is in agreement with the existence of the FTIR band at 685 cm^{-1}, which indicates significant octahedral cation substitution.

Additionally, the spectra from proximal samples also show a clear Fe(II) contribution that appears to be more intense than in the sample located away from the dome (MTO-14). This Fe(II) contribution is especially important in sample SE6M19, as it comprises ~30% of the overall Fe species of the sample. Furthermore, the spectrum of SE6M19 is very similar to that obtained by Beaufort & Meunier (1994) in a saponite sample from clay deposits in fractures of a metamorphic basement, suggesting that sample SE6M19 might be composed of a mixture of montmorillonite and Fe-rich saponite, in agreement with the FTIR spectra.

Finally, only the proximal samples SE6M19 and SE10M12 showed the presence of a magnetically ordered phase. The corresponding sextet, accounting for 3–4% of the total Fe species, has hyperfine parameters, ($\delta = 0.33$ mm/s; $2\varepsilon \approx -0.21$ mm/s; $H \approx 52$ T) consistent with hematite (α-Fe_2O_3) (Dyar *et al*., 2006). These results indicate that the majority of the Fe(III) ions are in the crystal structure of smectites substituting for octahedral Al.

The structural formulae calculated from TEM and EDX analyses are in good agreement with the FTIR and Mössbauer results, confirming that the Al-smectites from the Morrón de Mateo bentonite deposit were transformed into Fe-rich smectites, mainly because of the volcanic intrusion which raised the temperature and supplied solutions. These solutions were initially enriched in Fe(II), transforming original Al-montmorillonites into Fe-rich montmorillonites and beidellites. These smectites would transform into Fe-rich smectites with an intermediate composition between beidellite and saponite in those areas with intense water–rock interaction. Finally, Fe(II) was oxidized to Fe(III) when bentonites were exposed to more oxidizing conditions close to the surface.

CONCLUSIONS

The IR spectra of the fine fraction of bentonites from the Morrón de Mateo deposit indicate that smectites from proximal samples have greater Fe-contents than their counterparts from samples further away from the dome. These last samples show OH-stretching and bending bands typical of Al-rich montmorillonite, while spectra from proximal samples show bands characteristic of both Al-rich smectites and Fe-rich smectites. Furthermore, most spectra of the proximal samples contain typical Fe-rich saponite bands. The IR data are in agreement with the structural formulae calculated in previous studies, indicating the presence of Fe-rich montmorillonite and smectite with intermediate composition between beidellite and Fe-rich saponite.

https://doi.org/10.1180/clm.2018.1 Published online by Cambridge University Press

The Mössbauer data confirm that the Fe present in the fine fraction of bentonites is mainly located in the smectite structures, mainly as octahedral Fe(III). In two samples ~4% of total Fe is bound in hematite. Octahedral Fe(II) was identified as a minor component, except in one proximal sample where Fe(II) comprises 31% of the overall Fe species. This fact, and the characteristic FTIR bands, confirm the presence of Fe-rich saponite in this proximal sample.

Additionally, the Mössbauer spectra of proximal smectites contain two doublets characteristic of octahedral Fe(III). The much larger quadrupole splitting of one of these doublets indicates a much more distorted octahedral environment for this Fe(III) species, suggesting significant substitution of Al by Fe(III) in proximal samples.

The results confirm that alteration of smectites occurred in relation to the volcanic intrusion, which involved increase of temperature and supply of Fe-rich solutions responsible for the transformation of Al-montmorillonites into Fe-rich smectites.

ACKNOWLEDGMENTS

Financial support for this work was provided by ENRESA/CIEMAT and MINECO (Spain) through BARRA II (Contract number 774319) and MAT2015-64110-C2-1-P projects, respectively. The authors thank D. Tejela of Clariant Iberica Production, S.A. for providing the drill-core samples, and R. Saldaña for sample preparation. The authors also thank Martin Pentrák from the University of Illinois (USA) for the corrections, comments and suggestions that improved this work.

REFERENCES

Bancroft G.M. (1973) *Mössbauer Spectroscopy: An Introduction for Inorganic Chemists and Geochemists*. McGraw Hill, Maidenhead, Berkshire, England.

Beaufort D. & Meunier A. (1994) Saponite, corrensite and chlorite/saponite mixed-layered minerals and saponite in the Sancerre-Couy deep drill hole (France). *Clay Minerals*, **29**, 47–61.

Bergaya F., Brigatti M.F. & Fripiat J.J. (1985) Contribution of infrared spectroscopy to the study of corrensite. *Clays and Clay Minerals*, **33**, 458–462.

Bishop J.L., Murad E., Madejová J., Komadel P., Wagner U. & Scheinost A. (1999) Visible, Mössbauer and infrared spectroscopy of dioctahedral smectites: Structural analyses of the Fe-bearing smectites Sampor, SWy-1 and SWa-1. 11th International Clay Conference, June 1997, Ottawa, 413–419.

Bishop J.L., Madejová J., Komadel P. & Froeschl H. (2002) The influence of structural Fe, Al and Mg on the infrared OH bands in spectra of dioctahedral smectites. *Clay Minerals*, **37**, 607–616.

Brigatti M.F. (1983) Relationship between composition and structure in Fe-rich smectites. *Clay Minerals*, **18**, 177–186.

Caballero E., Reyes E., Yusta A., Huertas F. & Linares J. (1985) Las bentonitas de la zona sur de Cabo de Gata, Almería. Geoquímica y mineralogía. *Acta Geológica Hispánica*, **20**, 267–287.

Cardile C.M. & Johnston J.H. (1986) A ^{57}Fe Mössbauer spectroscopic study of montmorillonites: A new interpretation. *Clays and Clay Minerals*, **34**, 307–313.

Coey J. M. D. (1980) Clay minerals and their transformations studied with nuclear techniques: The contribution of Mössbauer spectroscopy. *Atomic Energy Review*, **18**, 73–124.

Cuadros J., Dekov V.M. & Fiore S. (2008) Crystal-chemistry of the mixed-layer sequence talc-talc-smectite-smectite from submarine hydrothermal vents. *American Mineralogist*, **93**, 1338–1348.

Dainyak L.G. & Drits V.A. (1987) Interpretation of Mössbauer spectra of nontronite, celadonite and glauconite. *Clays and Clay Minerals*, **35**, 363–373.

Dainyak L.G., Drits V.A. & Heifits L.M. (1992) Computer simulation of cation distribution in dioctahedral 2:1 layer silicates using IR-data: Application to Mössbauer spectroscopy of a glauconite sample. *Clays and Clay Minerals* **40**, 470–479.

De Grave E., Vandenbruwaene J. & Elewaut E. (1985) An^{57}Fe Mössbauer effect study on glauconites from different locations in Belgium and northern France. *Clay Minerals*, **20**, 171–179.

Delgado A. (1993) Estudio isotópico de los procesos diagenéticos e hidrotermales relacionados con la génesis de bentonitas (Cabo de Gata, Almería). PhD thesis, University of Granada, Spain, 413 pp.

Dyar M.D., Agresti D.G., Schaefer M.W., Grant C.A. & Sklute E.C. (2006) Mössbauer spectroscopy of earth and planetary materials. *Annual Review of Earth and Planetary Sciences*, **34**, 83–125.

Farmer V.C. (1974) The *Infrared Spectra of Minerals*. Monograph **4**. Mineralogical Society, London, 539 pp.

Farmer V.C. (1998) Differing effects of particle size and shape in the infrared and Raman spectra of kaolinite. *Clay Minerals*, **33**, 601–604.

Fernández-Soler J.M. (1992) El volcanismo calco-alcalino de Cabo de Gata (Almería). PhD thesis, University of Granada, Spain, 243 pp.

Fernández-Soler J.M. (2002) Thermal effect: Morrón de Mateo outcrop. Geological setting Memoir. *Barra II Project Report*, 41pp.

Goodman B.A., Russell J.D., Fraser A.R. & Woodhams F. W.D. (1976) A Mössbauer and I.R. spectroscopic

https://doi.org/10.1180/clm.2018.1 Published online by Cambridge University Press

study of the structure of nontronite. *Clays and Clay Minerals*, **24**, 53–59.

Goodman B.A. (1994) Mössbauer spectroscopy. Pp. 68–119 in: *Clay Mineralogy: Spectroscopic and Chemical Determinative Methods* (M.J. Wilson, editor). Chapman & Hall, London.

Guillaume D., Neaman A., Cathelineau M., Mosser-Ruck R., Peiffert C., Abdelmoula M., Dubessy J., Villiéras F. & Michau N. (2004) Experimental study of the transformation of smectite at 80 and 300°C in the presence of Fe oxides. *Clay Minerals*, **39**, 17–34.

Heller-Kallai L. & Rozenson I. (1981) The use of Mössbauer spectroscopy of iron in clay mineralogy. *Physics and Chemistry of Minerals*, **7**, 223–238.

Komadel P., Madejová J. & Stucki J.W. (1999) Partial stabilization of Fe (II) in reduced ferruginous smectite by Li fixation. *Clays and Clay Minerals*, **47**, 458–465.

Lantenois S., Lanson B., Muller F., Bauer A., Jullien M. & Plançon A. (2005) *Clays and Clay Minerals*, **53**, 597–612.

Maddock A.G. (1985) Mössbauer spectrometry in mineral chemistry. Pp. 141–208 in: *Chemical Bonding and Spectroscopy in Mineral Chemistry* (F.J. Berry & D.J. Vaughan, editors). Springer, Netherlands.

Madejová J., Komadel P. & Čičel B. (1994) Infrared study of octahedral site populations in smectites. *Clay Minerals*, **29**, 319–326.

Madejová J., Bujdák J., Petit S. & Komadel P. (2000) Effects of chemical composition and temperature of heating on the infrared spectra of Li-saturated dioctahedral smectites: (I) Mid-infrared region. *Clay Minerals*, **35**, 739–751.

Madejová J. & Komadel P. (2001) Baseline studies of The Clay Minerals Society source clays: infrared methods. *Clays and Clay Minerals*, **49**, 410–432.

Madejová J. (2003) FTIR techniques in clay mineral studies. *Vibrational Spectroscopy*, **31**, 1–10.

Moore D.M. & Reynolds R.C. (1997) *X-Ray Diffraction and the Identification and Analysis of Clay Minerals*. Oxford University Press, New York, 378 pp.

Murad E. (1988) Properties and behavior of iron oxides as determined by Mössbauer spectroscopy. Pp 309–350 in: *Iron in Soils and Clay Minerals* (J.W. Stucki, B.A. Goodman & U. Schwertmann, editors). Springer, Berlin.

Murad E. (2010) Mössbauer spectroscopy of clays, soils and their mineral constituents. *Clay Minerals*, **45**, 413–430.

Parra M., Delmont P., Ferragne A., Latouche C., Pons J.C. & Puechmaille C. (1985) Origin and evolution of smectites in recent marine sediments of the NE Atlantic. *Clay Minerals*, **20**, 335–346.

Pelayo M., García-Romero E., Labajo M.A. & Pérez del Villar L. (2011) Occurrence of Fe-Mg-rich smectites and corrensite in the Morrón de Mateo bentonite deposit (Cabo de Gata region, Spain): a natural analogue of the bentonite barrier in a radwaste repository. *Applied Geochemistry*, **26**, 1153–1168.

Pelayo M. (2014) Estudio del yacimiento de bentonita de Morrón de Mateo como análogo natural del comportamiento de la barrera de arcilla de un almacenamiento de residuos radiactivos. PhD thesis, Complutense University of Madrid, Spain, 311 pp.

Pelayo M., García-Romero E., Labajo M.A. & Pérez del Villar L. (2016) Evidence of montmorillonite/Fe-rich smectite transformation in the Morrónde Mateo bentonite deposit (Spain): implications for the clayey barrier behaviour. *Applied Clay Science*, **131**, 59–70.

Pérez del Villar L., Delgado A., Reyes E., Pelayo M., Fernández-Soler J.M., Cózar J.S., Tsige M. & Quejido A.J. (2005) Thermochemically induced transformations in Al-smectites: a Spanish natural analogue of the bentonite barrier behaviour in a radwaste disposal. *Applied Geochemistry*, **20**, 2252–2282.

Petit S., Caillaud J., Righi D., Madejová J., Elsass F. & Köster H.M. (2002) Characterization and crystal chemistry of a Fe-rich montmorillonite from Ölberg, Germany. *Clay Minerals*, **37**, 283–297.

Reyes E. (1977) Mineralogía y geoquímica de las bentonitas de la zona norte de Cabo de Gata (Almería). PhD thesis, University of Granada, Spain. 650 pp.

Rozalén M. (2004) Mecanismo y velocidad de disolución de montmorillonita en soluciones de electrolitos inertes. Influencia del pH y de la temperatura. PhD thesis, University of Granada, Spain. 299 pp.

Russell J. & Fraser A. (1994) Infrared methods. Pp. 11–67 in: *Clay Mineralogy: Spectroscopic and Chemical Determinative Methods* (M.J. Wilson, editor). Chapman & Hall, London.

Van der Marel H.W. & Beutelspacher H. (1976) *Atlas of Infrared Spectroscopy of Clay Minerals and their Mixtures*. Elsevier, Amsterdam, 396 pp.

Vantelon D., Pelletier M., Michot L.J., Barres O. & Thomas F. (2001) Fe, Mg and Al distribution in the octahedral sheet of montmorillonites. An infrared study in the OH-bending region. *Clay Minerals*, **36**, 369–379.

Wilkins R.W.T. & Ito J. (1967) Infrared spectra of some synthetic talcs. *American Mineralogist*, **52**, 1649–1661.

Wilson J., Cressey G., Cressey B., Cuadros J., Ragnarsdottir K.V., Savage D. & Shibata M. (2006) The effect of iron on montmorillonite stability. (II) Experimental investigation. *Geochimica et Cosmochimica Acta*, **70**, 323–326.

Zviagina B.B., McCarty D.K., Środon J. & Drits V.A. (2004) Interpretation of infrared spectra of dioctahedral smectites in the region of OH-stretching vibrations. *Clays and Clay Minerals*, **52**, 399–410.

https://doi.org/10.1180/clm.2018.1 Published online by Cambridge University Press